Mineralogy and Petrology (2003) 79: 167–191
DOI 10.1007/s00710-003-0238-3

Mineralogy and Petrology
Printed in Austria

Trace elements and cathodoluminescence of igneous quartz in topaz granites from the Hub Stock (Slavkovský Les Mts., Czech Republic)

A. Müller[1], **M. René**[2], **H.-J. Behr**[3], and **A. Kronz**[3]

[1] Natural History Museum, Department of Mineralogy, London, United Kingdom
[2] Institute of Rock Structure and Mechanics, Academy of Sciences of the Czech Republic, Prague, Czech Republic
[3] GZG, Göttingen, Germany

Received November 6, 2001; revised version accepted January 30, 2003
Published online June 2, 2003;
Editorial handling: A. Finch

Summary

Igneous quartz of the late-Variscan topaz-bearing granites from the Hub Stock (Slavkovský Les, Czech Republic) was investigated by cathodoluminescence (CL) and electron probe micro-analysis (EPMA) to demonstrate the intra-granular heterogeneity of growth patterns and trace element distribution in quartz. We show that EPMA is well suited for the *in situ* study of Al and Ti in zoned quartz, because of its high spatial resolution down to 5 μm in conjunction with the ability to combine spot analyses with CL imaging. In the quartz phenocrysts of the topaz granites high Ti is associated with blue luminescent growth zones. High Ti (>40 ppm) in quartz indicates a high crystallisation temperature and pressure. The groundmass quartz of the granites which is almost free of Ti, has higher Al than the phenocrysts which may reflect an increase of lithophile elements and water content in melt during the late magmatic stage. The occurrence of similar quartz phenocrysts in most of the late-Variscan granites and rhyolites of the Krušné Hory/Erzgebirge which intruded over a period of about 40 Ma points to a similar crystallisation environment and origin of the quartz phenocrysts in the lower to middle crust.

Introduction

Because of the limited mineral void space available in the quartz lattice and the relative high stability of Si–O bonds, it was long considered that the quartz

structure bears no genetic information. Some early studies, e.g. by the famous mineralogist *Frondel* (1934), noted that there is little chance of using compositional variations in quartz for genetic interpretations. Since then a number of studies have shown that trace element contents vary significantly within zoned quartz crystals as well as in quartz crystals from different environments (e.g., *Suttner* and *Leininger*, 1972; *Schrön* et al., 1988; *Blankenburg* et al., 1994).

The *in situ* trace element analysis of zoned quartz is technically difficult, because trace element concentrations in quartz are very low. Consequently, the relationship between quartz chemistry and petrogenesis is virtually unknown. Wavelength-dispersive electron probe micro-analysis (EPMA; *Lowenstern* and *Sinclair*, 1996; *Morgan* et al., 1998; *Mullis and Ramseyer*, 1999; *Van den Kerkhof* et al., 2001; *Müller* et al., 2000, 2002a, b, 2003), ion mass spectrometry (IMS; *Shimizu* et al., 1978; *Rovetta* et al., 1989; *Perny* et al., 1992; *Watt* et al., 1997), and laser-ablation inductively-coupled plasma-mass spectrometry (LA ICP-MS; *Larsen* et al., 2000; *Flem* et al., 2002) are *in situ* micro-beam techniques which are suitable for quantitative analysis of trace elements in quartz. These methods may provide *in situ* element data with a high sensitivity and good spatial resolution, allowing for the quantitative determination of element zoning within single crystals. Because of its better spatial resolution in conjunction with the ability to combine spot analyses with cathodoluminescence (CL) imaging, EPMA proved the most reliable *in situ* method for obtaining quantitative trace element data of quartz at concentrations in excess of a few 10's of ppm and at the $<10\,\mu m$ scale (*Müller* et al., 2003). For that reason, in this study EPMA is applied for the determination of trace element distribution in igneous quartz.

Electron-excited luminescence, or cathodoluminescence (CL), is a sensitive method for revealing growth zoning, alteration patterns, grain shapes and different generations of quartz, which are not distinguishable in transmitted or polarised light (e.g. *Seyedolali* et al., 1997; *D'Lemos* et al., 1997; *Watt* et al., 1997; *Müller* et al., 2000, 2002a, b; *Götze* et al., 2001; *Holness* and *Watt*, 2001). Spatial variations of CL properties reflect structural and chemical variations within quartz crystals, which are related to crystal growth zones or alteration patterns. CL colour and intensity in quartz are generally controlled by activator and sensitizer elements (extrinsic lattice defects), such as Al, Ti, Fe, Mn, Ge, Li, Na, and H, and intrinsic defects (e.g., oxygen and silicon vacancies) (e.g., *Sprunt*, 1981; *Waychunas*, 1988; *Perny* et al., 1992; *Stevens Kalceff* and *Phillips*, 1995; *Pagel* et al., 2000; *Götze* et al., 2001). Al^{3+}, Ti^{4+}, Fe^{3+}, and Ge^{4+} substitute for Si^{4+} and monovalent ions, such as H^+, Li^+, Na^+, and K^+ act as compensators of the electric charge at interstitial positions (e.g. *Bambauer*, 1961; *Dennen*, 1965; *Lehmann*, 1975; *Lehmann* and *Bambauer*, 1973; *Maschmeyer* and *Lehmann*, 1983; *Weil*, 1984; *Bahadur*, 1993). Therefore, CL can be an indirect indicator of trace element distributions in quartz. Despite considerable benefits of the phenomenological investigation of the CL of quartz, the relationship between CL properties, trace elements, and petrogenesis is still not understood.

Compositional variations between growth zones in igneous quartz are caused by fluctuations in growth and diffusion rates in the melt through the crystal-melt boundary layer. Growth and diffusion rates are controlled either by a self-organising

intrinsic mechanism or by an extrinsic mechanism involving physical or chemical changes within the bulk system, such as crystal settling, large-scale convection, magma mixing, ascent velocity and related temperature and pressure changes (e.g. *Sibley* et al., 1976; *Shore* and *Fowler*, 1996). The challenge, however, is to relate the different patterns of zoning to specific genetic processes.

This study is focused on igneous quartz from the topaz-bearing granites of the Hub Stock hosting the Krásno Sn-W deposit (Slavkovský Les Mountains, Czech Republic). Aims of this study are:

- the high resolution (~10 μm) trace element determination within quartz crystals by electron microprobe (EPMA),
- to illustrate links between trace element distribution and CL of quartz,
- to relate quartz growth patterns identified by CL to magma genetic processes,
- to discuss the petrogenetic significance of trace element distribution,
- and finally, to present some geological implications for late-Variscan magmatism.

Geological setting and petrography

The Krušné Hory/Erzgebirge batholith extends over an area of about 6000 km^2 and belongs to the largest Variscan granite bodies in the Bohemian Massif (Fig. 1). Topaz-albite granites that usually form granite stocks are traditionally related to the younger intrusive complex (YIC) of the Krušné Hory/Erzgebirge batholith (*Fiala*, 1968; *Lange* et al., 1972). However, the topaz-albite granites of the Hub Stock form part of a complicated stock structure of topaz-albite granites, which are associated with the upper part of the Krásno Sn-W ore deposit (*Jarchovský* et al., 1994; *René*, 1998). Topaz-albite granites in this part of the Slavkovský Les Mts. are part of the Krudum massif that forms a relatively independent magmatic body in the SW part of the Krušné Hory/Erzgebirge batholith.

The emplacement of the granite stock was associated with intensive tectonic deformation of slightly migmatized biotite paragneisses in the pre-Variscan basement. Intrusive breccias described in detail by *Jarchovský* and *Pavlů* (1991) and *Seltmann* et al. (1992) occur in the upper part of the Hub stock. The breccias are cemented by topaz-albite microgranites (Fig. 2), which form dykes penetrating the gneiss roof up to 100 m away from the contact (*Jarchovský* and *Pavlů*, 1991).

Topaz-albite microgranites (sample Ju-20) are aplitic (grain size: 200–500 μm) and rarely porphyritic. The microgranitic rocks include K-feldspars that are several millimetres in size as well as bipyramidal quartz (1.5–3 mm). The groundmass of the microgranitic rocks is composed of anhedral quartz, albite, Li-mica, K-feldspar, and primary topaz. Topaz-albite granites of the Hub stock are mostly medium-grained varieties, locally accompanied by fine-grained, porphyritic topaz-albite granite.

The porphyritic topaz-albite granite (sample Ju-10) has an equigranular groundmass (50–100 μm) of anhedral quartz, albite (An_{03-05}), K-feldspar, Li-mica, topaz, muscovite, and accessory minerals (apatite, zircon, rarely monazite, Nb-Ta rutile and other accessories, see Table 1). The phenocryst population is dominated

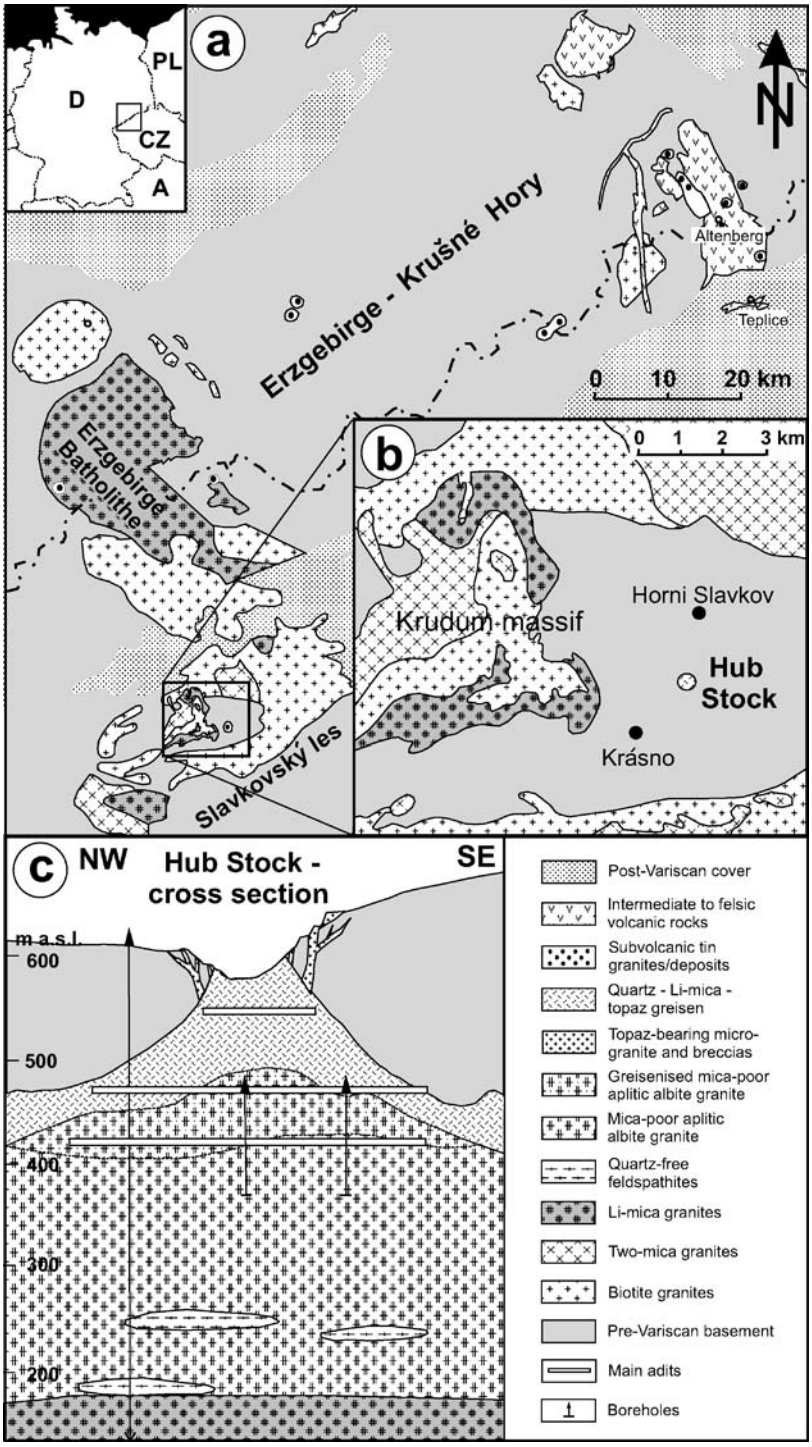

Fig. 1. Geological setting of the Hub stock. **a**, **b** Geological map of the Krušné Hory/Erzgebirge with the distribution of late-Variscan granites and the location of the Hub stock. **c** Simplified cross-section through the Hub stock according to *Jarchovský* (2001)

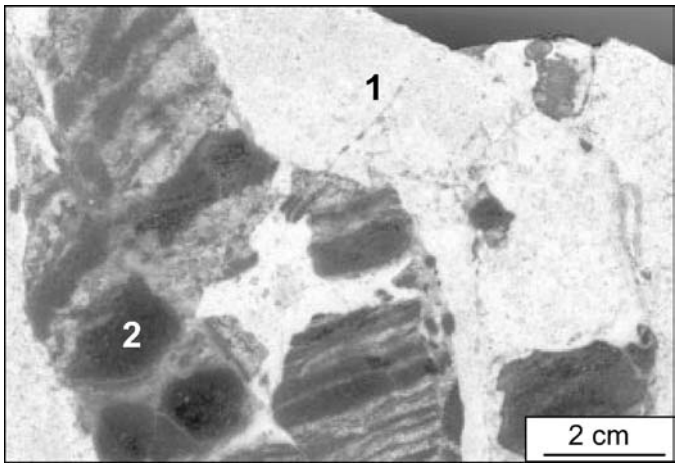

Fig. 2. Polished hand specimen of intrusion breccia from the Hub stock open pit consisting of angular gneiss fragments (2), which are cemented by leucocratic topaz-albite microgranite (1). The microgranite of small-scale apophyses is almost free of phenocrysts, because the phenocrysts could not pass the fine network of cracks

Table 1. *Mineralogical composition and petrographic features of topaz-bearing granites of the Krudum massif*

Granite types	Macroscopic features	Microscopic features	Rock-forming minerals	Accessory minerals
Topaz-albite granite of the Cista type (Ju-10)	Medium grained, equigranular to porphyric, grey, greyish white and whitish	Grainsize of individual minerals 1–3 mm, granitic texture	Quartz, albite (An_{0-10}), Li-mica, K-feldspar, topaz	*Apatite, Zircon*, Monazite, Xenotime, Nb-Ta-rutile, Columbite, Uraninite, U-Ca-phosphate, As-crandallite
Topaz-albite microgranite (Ju-20)	Very fine grained matrix of polymict intrusion breccias	Very fine to aphanitic texture	Albite, K-feldspar, quartz, Li-mica, topaz	*Apatite*, *Cassiterite,* Nb-Ta-rutile, Monazite, Zircon, Xenotime, Brabantite, Gahnite, Nigerite

by bipyramidal quartz (1.5–3 mm), platy Li-mica ($\leq$3 mm), and sparse K-feldspar up to two centimetres in size. The two textural varieties may represent different granitic facies of approximately the same age, the origin of which was controlled by local pressure conditions during emplacement and crystallisation (*René*, 1998). Mineralogical composition and petrographic features of topaz-bearing granites and their whole rock chemistry are shown in Table 1 and 2, respectively.

Table 2. *Chemical composition of topaz-bearing granites from the Hub stock*

wt.%	Ju-10	Ju-20
SiO_2	74.59	72.74
TiO_2	0.15	0.04
Al_2O_3	13.51	14.82
Fe_2O_3	0.13	0.09
FeO	1.14	0.68
MnO	0.04	0.06
MgO	0.29	0.13
CaO	0.54	0.51
Na_2O	2.80	4.66
K_2O	5.03	3.82
P_2O_5	0.14	0.32
L.O.I.	1.00	1.50
F	0.23	1.52
Total	99.59	100.89
ppm		
Ba	159	110
Rb	456	1590
Sr	44	29
Zr	111	17
Nb	15	47
Y	38	14
Zn	45	582
Sn	15	357
Th	15.4	8.7
U	22.7	9.3

Methodology

Cathodoluminescence (CL)

CL investigations were carried out using the *Simon-Neuser's* "hot-cathodoluminescence-microscope" HC2-LM (*Neuser* et al., 1995) at the GZ Göttingen. The acceleration voltage was 14 keV and the filament current 0.18 mA. CL spectra were recorded with a triple-grating (100, 1200, and 1800 lines mm^{-1}) spectrograph TRIAX 320 equipped with a liquid N_2-cooled charge coupled device (CCD) camera. The system is well suited for applications at very low signals, such as the CL of quartz. The 100-lines mm^{-1} grating was used to detect the emitted spectra between 400 and 950 nm (3.1 and 1.4 eV), whereas the 1200 lines mm^{-1} grating provided high-resolution spectra of 70 nm-wide sectors. The latter allows the exact energy of single CL emission bands to be detected. The integration time of spectrum acquisition was 20 s for the 100 lines mm^{-1} grating and 30 s for the 1200 lines mm^{-1} grating. The spectra were corrected for the total instrument response.

The peak fitting of quartz CL spectra was carried out to determine the energy and intensity of individual emission bands, which usually have a Gaussian shape if

the spectrum is plotted in energy space (eV). The position, width, and height of the Gaussian curves were calculated and adjusted in such a way that the sum of the individual components corresponds to the recorded CL spectrum. On the data base of about 200 quartz CL spectra a peak fitting procedure was developed, which allows deconvolution of the typically broad and overlapping emission bands of quartz spectra (*Müller*, 2000; *Müller* et al., 2002b). This procedure is based mainly on observations of quartz spectra and it is not a simple mathematical fitting.

The application of an electron microprobe equipped with a CL detector (SEM-CL) allows the analysis of trace element distribution in relation to CL structures. Generally, CL detectors attached to a SEM provide monochromatic (grey scale) images of the CL structures within quartz crystals. The used JEOL SM-CLD40 R712 photo-multiplier records photon emissions between 200 to 900 nm and is most sensitive at wavelengths around 600 nm. Images were collected from the JEOL system using a beam voltage of 30 kV, a filament current of 200 nA, slow beam scan rates of 20 s per image, and a image resolution of 1024×860 pixels and 256 grey levels. Examination of luminescence colours of investigated quartz by optical CL reveals that dark contrasted areas of quartz SEM-CL images correspond to red to reddish brown CL colours and bright areas correspond to blue to violet colours. SEM-CL imaging was performed prior to and after EPMA analysis. The measurement points can thus be located exactly in relation to the CL structures. The grey scale profiles along measured trace element profiles within quartz crystals were processed from the SEM-CL images using the software Optimas 6.0.

Electron probe micro-analysis (EPMA)

Trace element abundances of Al, Ti, K, and Fe in quartz were determined using a JEOL 8900 RL electron microprobe at the GZ Göttingen equipped with 5 WD detectors. The following standards were used for the analysis: synthetic Al_2O_3 (52.92 wt% Al), orthoclase, Lucerne, Switzerland (12.18 wt% K), synthetic TiO_2 (59.95 wt% Ti), and hematite, Rio Marina, Elba (69.94 wt% Fe). Raw analyses were converted into concentrations, after making appropriate matrix corrections using the phi-rho-z method of *Armstrong* (1991, 1995). For high precision and sensitivity, a high beam current of 120 nA, a beam diameter of 7 µm, and counting

Table 3. *Limits of detection (LOD). The average background (BG) is the total acquired counts for each element using 120 seconds counting time on each side of the peak (20 kV accelerating voltage and a beam current of 120 nA)*

Element	Counting time peak [s]	Each BG [s]	Average BG total [cts]	Factor (lin. calib.)	LOD by n = 54 measurements		LOD by single measurement average	
					$I_{LOD} = 2.01 * \sigma_{BG}$ [cts]	C_{LOD} [ppm]	$I_{LOD} = 3 * \sqrt{BG}$ [cts]	C_{LOD} [ppm]
Al	240	120	110600	0.013	4537	60	997	13
K	240	120	17900	0.024	376	9	401	10
Ti	240	120	40900	0.022	728	16	607	13
Fe	240	120	43360	0.024	637	15	625	15

rates of 240 s for Al, Ti, K, and Fe on the characteristic x-ray line and 120 s for each background signal were chosen. Backgrounds were measured on both sides of the peak. Curvature of the background signal for Al was taken into account.

Limits of detection (LOD) were calculated from 54 background measurements with 95% confidence utilising the Student's *t*-distribution according to the following equation (Table 3):

$$I_{LOD} = \mathrm{t_z}\,(\mathrm{P};\mathrm{f})\,\sigma_{\mathrm{BG}}$$

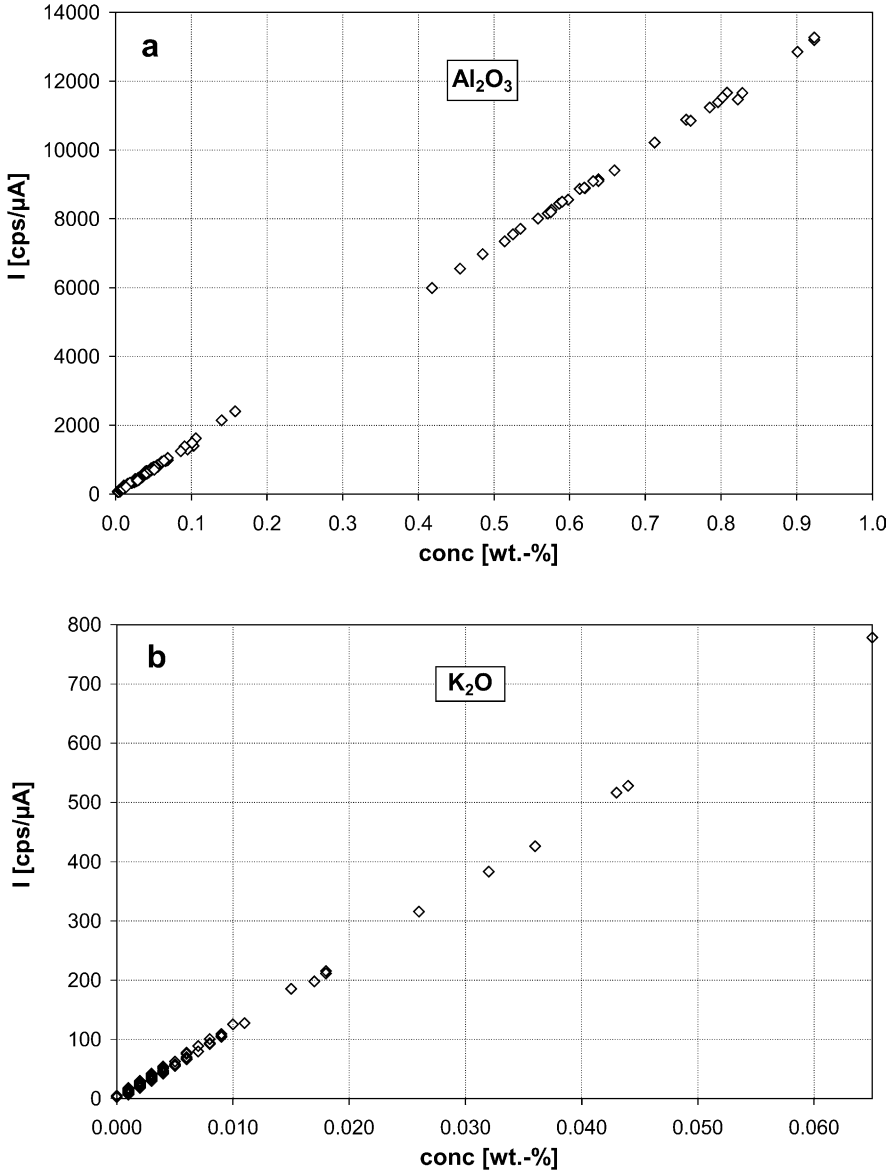

Fig. 3. Plots of the total intensity vs. concentration (wt.%) of Al_2O_3 (**a**) and K_2O (**b**) showing a good linearity. The factor of the linear calibration is used for the calculation of C_{LOD} (see Table 3)

where I_{LOD} = intensity of the LOD [cts]; σ_{BG} = standard deviation of the average background; t_z (P; f) = the Student's t for binomial limitation determined by the confidence P and the degrees of freedom $f = n - 2$, where n is the number of background measurements. The Student's t with 95% confidence amounts to 2.01 for 54 background measurements.

For comparison also the common method for calculating LOD, given by:

$$I_{LOD} = 3 \cdot \sqrt{BG}$$

for a single measurement was estimated.

BG are the total accumulated counts of the background signal (''LOD by single measurement''). Both methods give comparable results, but we prefer the random sampling using Student's t-test. The latter is more sensitive to systematic errors and the occurrence of drift-phenomena. The higher value of LOD for Al by multiple background measurement is due to a different shift of the total signal during acquisition time.

The concentration of LOD C_{LOD} is calculated using the factor of the linear calibration of total intensity vs. concentration of an element (Fig. 3, Table 3):

$$C_{LOD}\,[\text{ppm}] = \text{factor} * I_{LOD}$$

Due to the constant composition of the matrix SiO_2, there would be no change in the ZAF-factors, hence a linear calculation is reliable.

Detection limits are 60 ppm for Al, 16 ppm for Ti, 10 ppm for K, and 15 ppm for Fe at the primary beam conditions quoted. Trace element measurements were carried out as line scans yielding distribution profiles.

There are several reasons why the concentrations of Al, Ti, K and Fe were determined. Al^{3+} and Ti^{4+} most frequently substitute for Si^{4+} in quartz, and thus may strongly influence the CL of quartz (e.g., *Ramseyer* and *Mullis*, 1990; *Perny* et al., 1992; *Müller* et al., 2000). K^+ was selected as representative of the interstitial ions, because the detection limit of Na^+ (~80 ppm) was higher than the typical concentrations and Li^+ cannot be measured by EPMA. *Müller* et al. (2003) show, that K^+, Li^+, and Na^+ correlate positively in quartz of different origin and, therefore, K^+ is representative for the three monovalent ions. Fe and Mn are important CL activators and quenchers in silicates (*Marshall*, 1988). However, the concentration of Mn was far below the detection limit of 15 ppm.

Quartz growth patterns

The quartz phenocrysts (qz1) of both topaz-albite granite varieties (samples Ju-10 and Ju-20) exhibit a complex and generally similar growth pattern contrasted by different shades of blue, violet, and red-brown CL (Figs. 4a, b, d). However, there are a few large phenocrysts (>3 mm) which record a more complex growth probably reflecting a longer crystallisation history (Fig. 4c). Additionally, we identified a common population of magmatic quartz (200–500 µm in size) besides the phenocrysts (qz1) and the groundmass quartz (qz3) in the topaz-albite granite (Ju-10; Figs. 4a, 5a, 5b). Similar to the large phenocrysts, the qz2 population exhibits a dipyramidal β-quartz habit and growth zoning. The comparison of CL colour and growth zoning shows that nucleation and growth of the microphenocrysts (qz2)

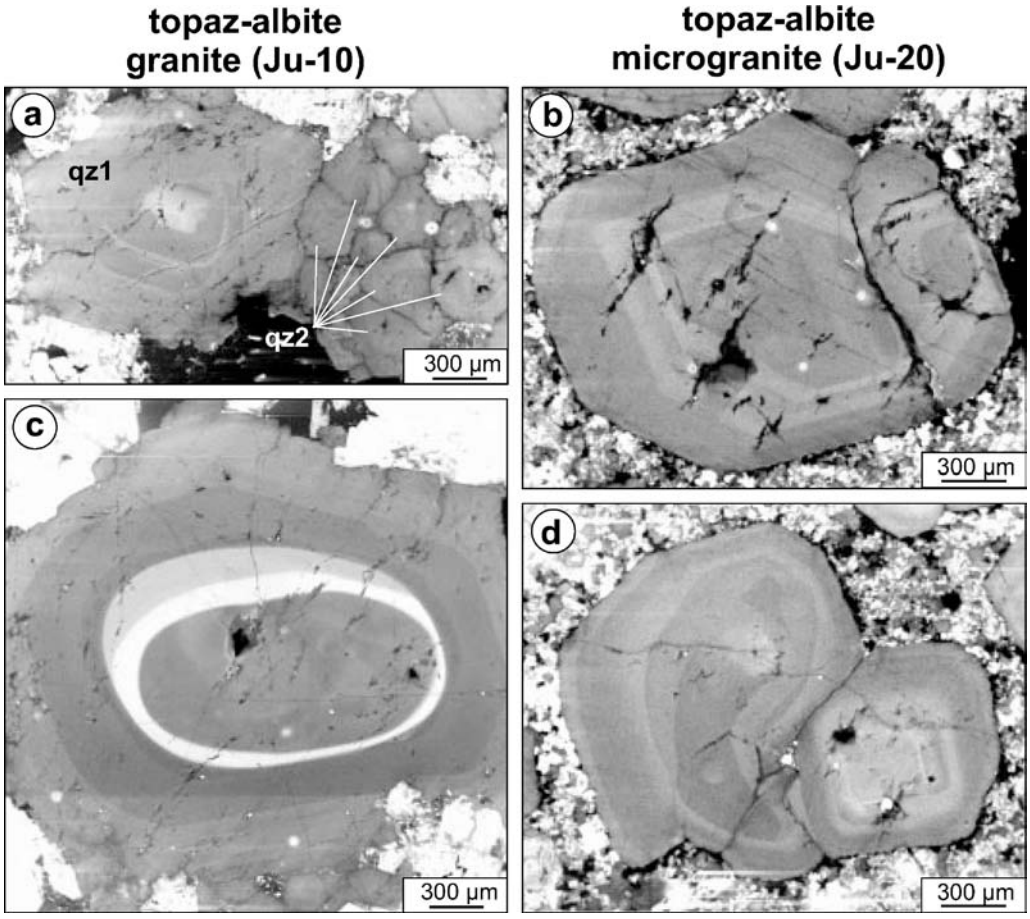

Fig. 4. SEM-CL images of quartz in the topaz-bearing granites of the Hub stock. **a** Zoned phenocryst (qz1) next to a cluster of weakly zoned microphenocrysts (qz2). **b** Zoned phenocryst in the microgranite. **c** Large phenocryst (~3 mm) with bright (blue), resorbed (rounded) growth zones. **d** Two adjacent phenocrysts of the microgranite. The phenocryst on the right impeded the growth of the phenocryst on the left. The small, irregular black areas in all quartz crystals are domains of post-magmatic, neocrystallised quartz

starts with the growth of the outer zone of qz1 (Figs. 5a, b). Both phenocryst populations form a maximum in the grain size distribution plot: qz1 at 2 mm and qz2 at 0.4 mm. The 0.4-mm-population microphenocryst will now be designated (qz2). Both the phenocrysts and microphenocrysts are overgrown by younger groundmass quartz.

Growth zoning in qz1 and qz2 includes step (compositional) zoning (*Allègre* et al., 1981) and oscillatory zoning with β-quartz habit (Fig. 4). Additionally, resorption surfaces and growth embayments occur in qz1 phenocrysts (*Kozlowski*, 1981; *Schneider*, 1993; *Müller* et al., 2000; Figs. 5c, d, e). Low-amplitude, fine-scale oscillatory zoning (2–20 µm width) is developed within super-ordinate, high-amplitude step zoning (50–1000 µm width). Step zones end with an abrupt change of CL colour whereby the outer oscillatory zones of the step zone or entire step zones are truncated resulting in rounding of crystals (Figs. 4c and 5c). In contrast,

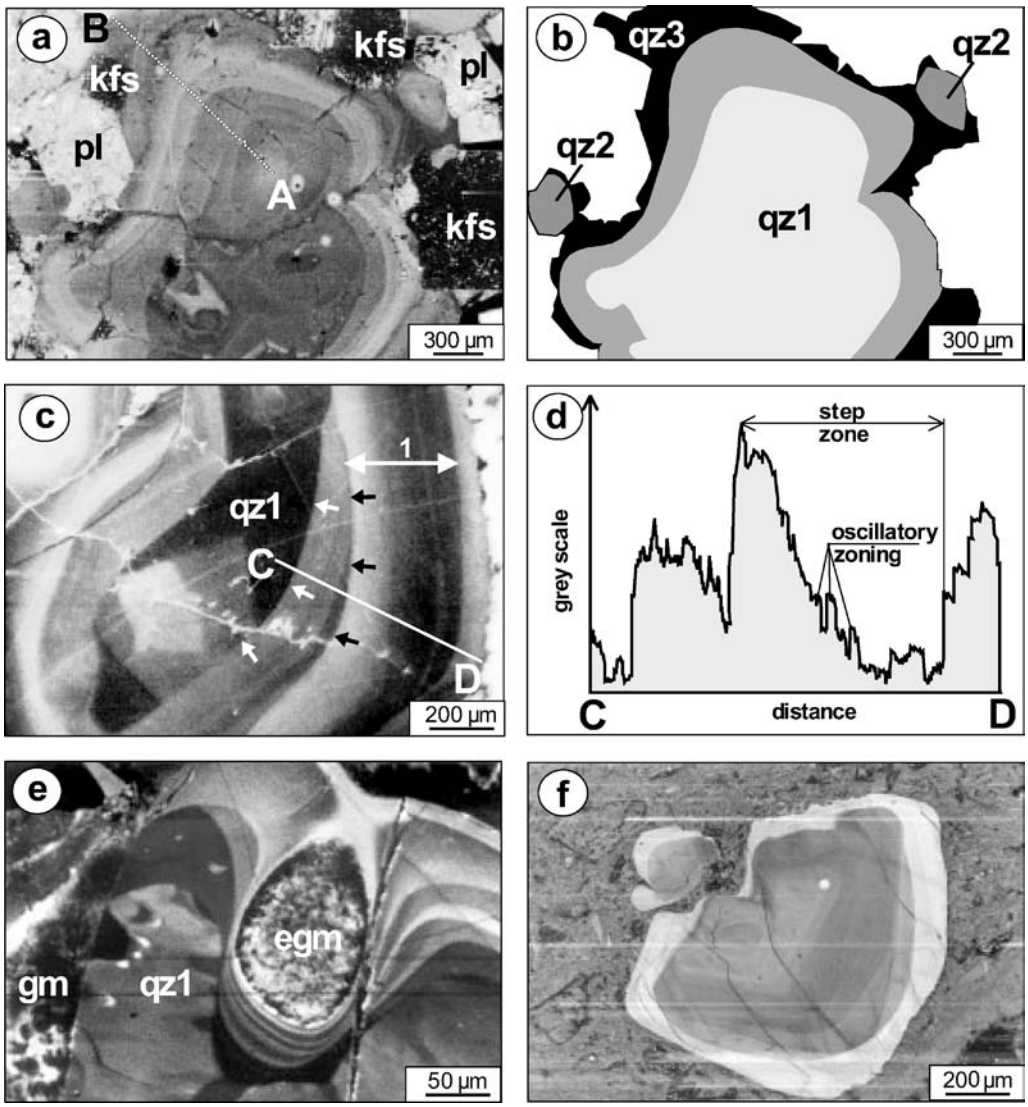

Fig. 5. **a** SEM-CL image of quartz in sample Ju-10. The line A–B shows the position of the trace element profile which is plotted in Figs. 7a, c, and e. **b** Scheme of quartz populations, distinguishable in the SEM-CL image 4a: zoned phenocryst (qz1), zoned microphenocrysts (qz2), and groundmass quartz (qz3), developed as overgrowths. Nucleation and growth of qz2 started with the growth of the outer step zone of qz1. **c** SEM-CL image of a phenocryst in sample Ju-20. The step zones (1) are bordered by resorption surfaces (arrowed). Within the step zones fine-scale oscillatory zoning is developed. Three main resorption episodes are recorded in the zoning pattern. **d** Grey scale profile across the quartz phenocryst shown in Fig. 5c (C–D). High grey scale corresponds to blue CL and low grey scale to red-brown CL. Within a step zone, the grey scale (blue CL) tends to decrease in the growth direction. **e** SEM-CL image of a phenocryst (qz1) with growth impediment. The zoning fits the shape of the lobate embayment. During further growth groundmass minerals (gm) within the embayment were enclosed (egm). **f** Zoned quartz phenocryst from the Teplice Rhyolite (Eastern Krušné Hory/Erzgebirge)

the zoning adapts to the shape of lobate and drop-like embayments (Fig. 5e). Therefore, it is traditionally interpreted as growth impediments (*Laemmlein*, 1930; *Kozlowski*, 1981; *Lowenstern*, 1995).

The existence of euhedral quartz phenocrysts in granites showing CL-contrasted growth zoning is currently not known to be common and has been described in only a few cases (*Seltmann*, 1994; *D'Lemos* et al., 1997; *Müller* et al., 2000, 2001, 2002a, b). Furthermore, the growth zoning of these granitic phenocrysts is similar to growth zoning and CL colours of phenocrysts observed in Permo-carboniferous rhyolites of the Krušné Hory/Erzgebirge (Fig. 5f). In contrast the groundmass quartz (qz3) overgrowing qz1 and qz2 is free of growth zoning and exhibits a red-brown CL (Fig. 5b).

Quartz formed during post-magmatic or late-magmatic alteration can easily be distinguished from the above-described magmatic quartz. Post-magmatic recrystallisation textures (fluid saturation textures, grain blasteses, cannibalising; e.g. *Müller* and *Seltmann*, 1999), and metasomatic quartz textures formed by hydrothermal processes show typically either weak red-brown or no luminescence. They are not the subject of this study.

Quartz CL colours and trace element distribution

The spectral response of the CL of quartz in the range of visible light is composed of 9 emission bands between 1.4 and 3.1 eV listed in Table 4 (Fig. 6). The intensity of the emission bands changes with the exposure time of electron radiation, whereby the blue emission decreases and the red emission increases, indicating the decay or creation of luminescence centres, respectively. The bluish CL colours obtained from phenocrysts within both granitic varieties are similar (Figs. 6a and b), whereas the CL spectra of groundmass quartz show a dominance of the red emission (Fig. 6c).

Growth zones with blue CL within the phenocrysts (qz1 and qz2) have up to 70 ppm Ti (Figs. 7a and b). Ti contents rise continuously with increasing blue CL (Fig. 8a). The Ti concentration varies between different luminescent growth zones, which may indicate that the Ti variation is responsible for the CL-contrasted zoning within qz1 and qz2. *Müller* et al. (2002b) show that high Ti concentrations in quartz correlate positively with the blue 2.96 eV emission band. This emission band represents the relatively stable part of the blue emissions (see Table 4). However, the electron bombardment and related thermal quenching probably cause the slight decrease of the CL signal during radiation. The distinct association between growth zones and Ti distribution suggests, that the analysed Ti is mainly structurally incorporated in the quartz lattice. Rutile micro-inclusions could not be detected by back-scattered electron imaging. However, it is generally not clear whether Ti is a CL activator or sensitizer (*Marshall*, 1988; *Götze*, 2000) and, therefore, the defect directly responsible for the 2.96 eV emission cannot be defined yet.

Phenocryst quartz (qz1 and qz2) has Al contents between 170 and 270 ppm, whereas groundmass quartz (qz3) carries 250–370 ppm (Fig. 7c). Al concentrations >400 ppm correlate with K. Non-luminescent secondary quartz of neocrystallised domains has Al contents <150 ppm (see Fig. 4). Al generally behaves

Table 4. *CL emission bands between 1.4 and 3.1 eV determined in igneous quartz of the topaz-bearing granites from the Hub stock*

CL band position (eV)	1.73 ± 0.02	1.84 ± 0.01	1.96 ± 0.02	2.15 ± 0.02	2.47 ± 0.02	2.58 ± 0.01	2.68 ± 0.01	2.79 ± 0.01	2.96 ± 0.02
Half width (eV)	0.3 ± 0.02	0.22 ± 0.01	0.22 ± 0.02	0.38 ± 0.01	0.3 ± 0.03	0.18 ± 0.005	0.23 ± 0.01	0.26 ± 0.01	0.3 ± 0.02
CL colour	red	red	red	yellow	green	blue	blue	blue	blue-violet

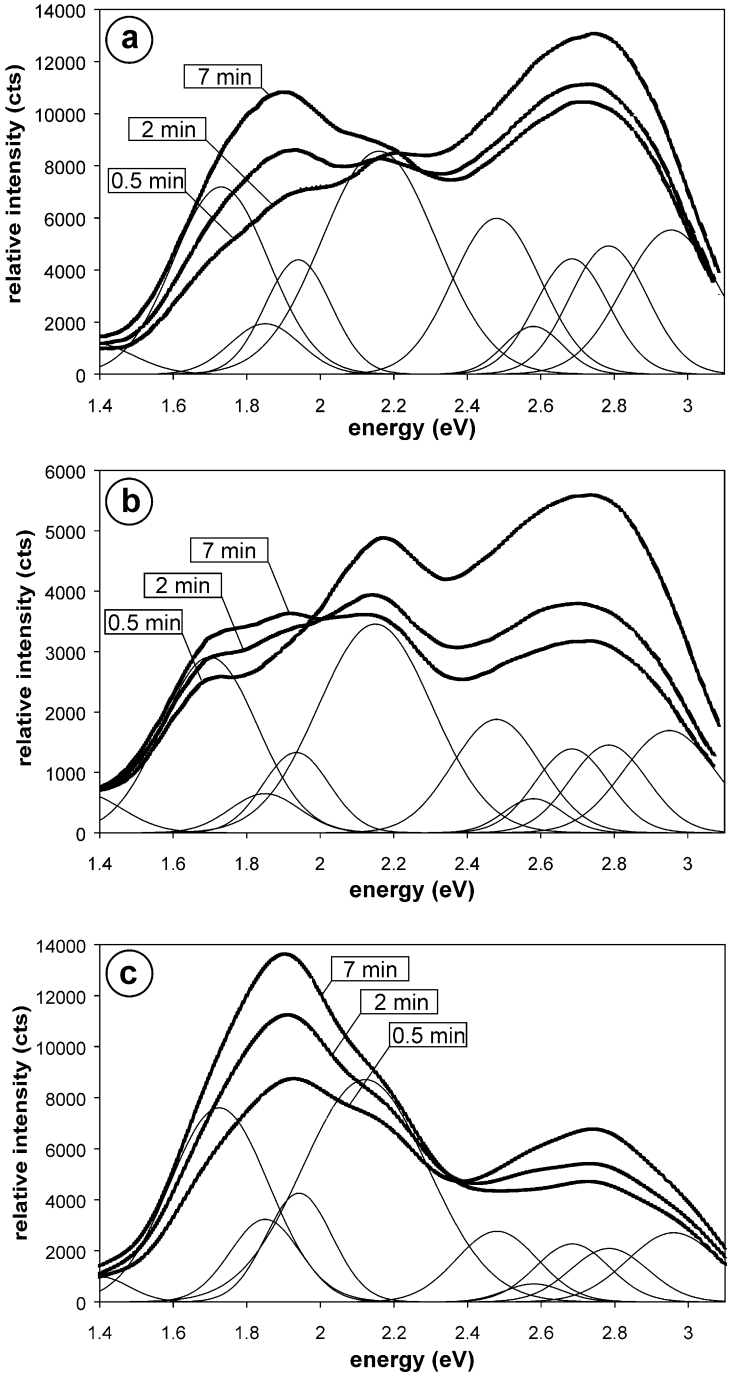

Fig. 6. CL spectra of **a** violet luminescent quartz phenocryst of sample Ju-10, **b** violet luminescent quartz phenocryst of sample Ju-20, and **c** red-brown luminescent groundmass quartz (Ju-10). The spectra were recorded after 30 s, 2 min, and 7 min electron radiation. The 7-min-spectra are fitted with Gaussian curves. Each Gaussian curve represents a single emission band

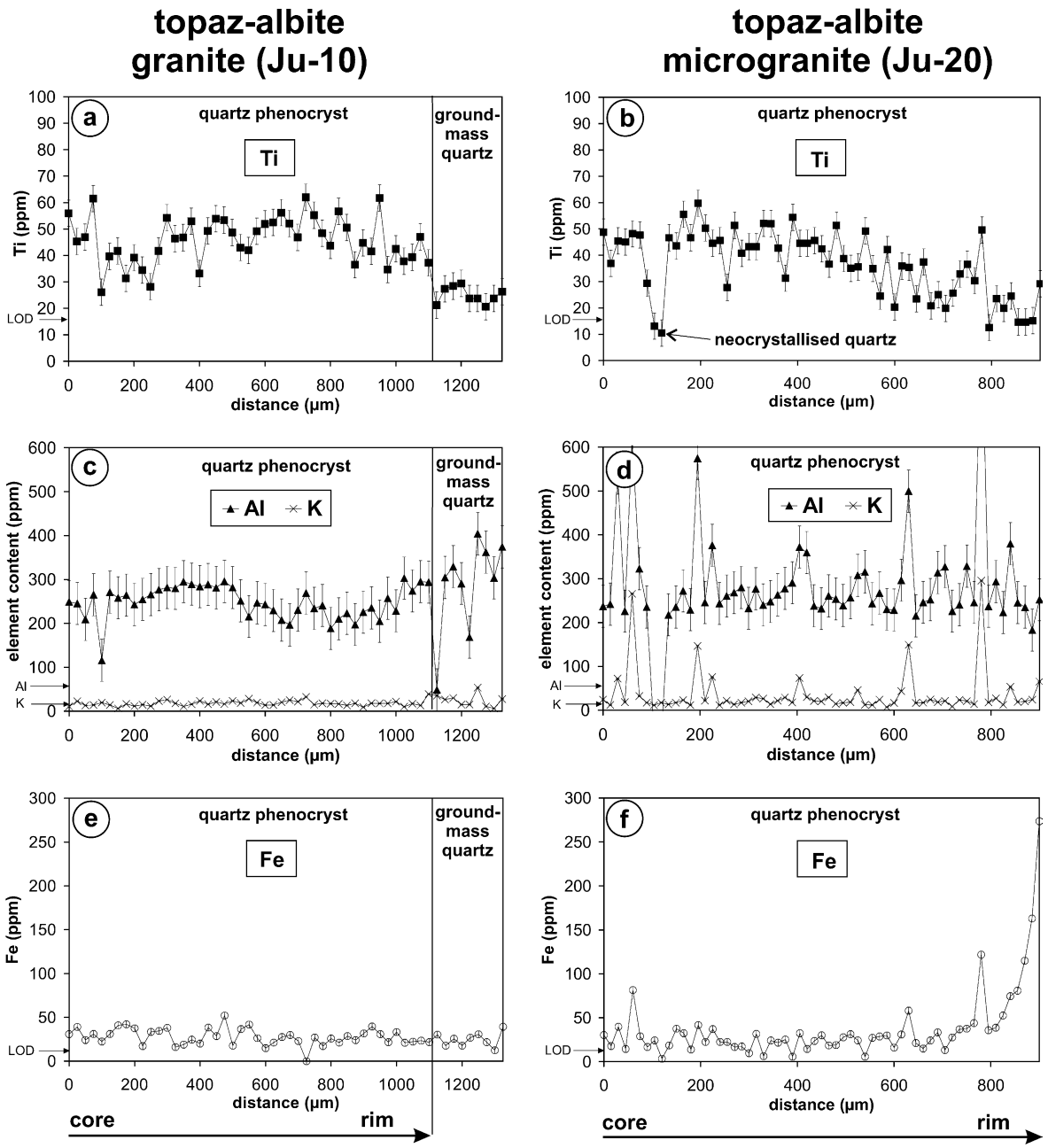

Fig. 7. Trace element line scans in quartz. Lower Ti and higher Al are characteristic for the groundmass quartz. Domains of post-magmatic neocrystallised quartz between 100 and 130 µm in **b**, **d**, and **f** are depleted in Ti, Al, Fe and K. Arrows at the axis of ordinate mark the limits of detection (LOD)

antipathetically to Ti; low and high concentrations occur in the blue and red-brown luminescent quartz, respectively. The weak red-brown luminescent groundmass quartz has the highest Al content (qz3; Fig. 8b). This observation is in contrast to CL and trace element associations of hydrothermal quartz. *Ramseyer* and *Mullis*

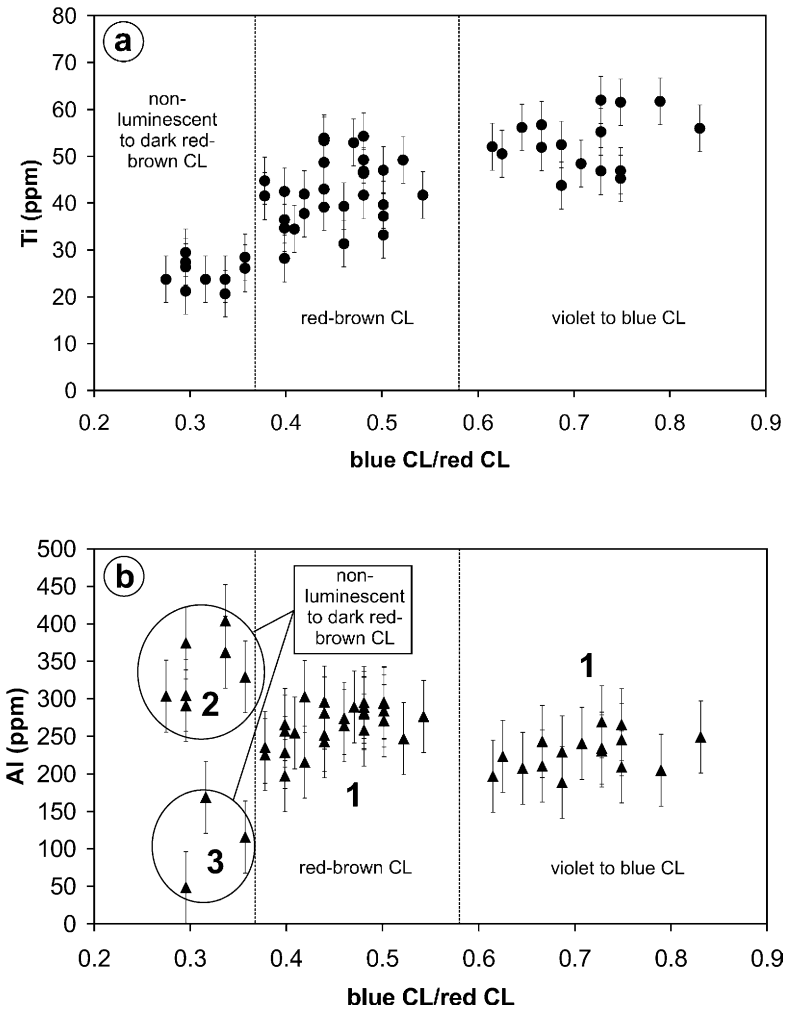

Fig. 8. **a** Ti versus CL signal plot of the zoned quartz phenocryst (qz1, Ju-10). The "red CL" is the sum of the Gaussian curve areas from the 1.73, 1.84, 1.96, 2.15 eV emissions and the "blue" CL is sum of the Gaussian curve areas from the 2.47, 2.58, 2.68, 2.79, 2.96 eV emissions. The "blue CL/red CL" ratio was interpolated for each point analysis from the grey scale obtained from the SEM-CL image (see Fig. 5a). **b** Al concentration of the quartz phenocryst (1), the groundmass quartz (2), and the neocrystallised (post-magmatic) quartz (3). The groundmass quartz has relative high Al in comparison to the quartz phenocryst and the neocrystallised quartz

(1990) and *Perny* et al. (1992) reported high Al and Li concentrations in blue luminescent zones of hydrothermal quartz, but this blue CL may not be caused by the blue 2.96 eV emission band. According to *Siegel* and *Marrone* (1981), *Griscom* (1985), and *Stevens Kalceff* and *Phillips* (1995), the red CL emission around 1.96 eV is related to non-bridging oxygen hole centre (NBOHC). OH^- and/or adsorbed H_2O are two possible precursors of the NBOHC. The increase in emission during electron radiation is explained by radiolysis of hydroxyl groups and/or adsorbed H_2O of the quartz lattice, which leads to the formation of NBOHC. Hydroxyl groups and adsorbed H_2O acting as charge compensators for

Al^{3+} defects beside Li^{+}, K^{+}, or Na^{+} (*Bambauer* et al., 1963; *Maschmeyer* and *Lehmann*, 1983; *Kronenberg* et al., 1986; *Bahadur*, 1993). *Stenina* et al. (1988) and *Stenina* (1995) stated that substitutional M^{3+} (e.g., Al^{3+} and Fe^{3+}) and related compensating M^{+} (Li^{+}, Na^{+}, and K^{+}) create water-bearing defects in the form of $2[SiO_3]^{+}$–H_2O–M^{+}–$2[M^{3+}O_4]^{-}$. This association of Al and hydroxyl groups and/or adsorbed H_2O may explain the weak correlation of Al with the red emission. On the other hand, the complex defect structure implies that its CL emission is non-trivial and should not cause a simple correlation of Al abundance with CL emission. The correlation of high Al with relative high K fits with the general assumption that K^{+} acts as charge compensator for Al^{3+}. However, the high concentrations suggest that both elements occur in sub-microscopic defect clusters. The larger ion radius of Al^{3+} ($r = 0.47$ Å) compared to Si^{4+} ($r = 0.34$ Å) explains why high amounts of structurally incorporated Al^{3+} (>400 ppm) should cause an extreme deformation and weakening of the quartz lattice.

The Fe content varies near the detection limit between 10 and 30 ppm which allows no interpretation (Figs. 7e and f). However, the Fe concentration increases up to 260 ppm towards the grain boundary, suggesting a diffusion profile of Fe in the quartz lattice. This crystal rim shows no change in CL properties. *Pott* and *McNicol* (1971) and *Kempe* et al. (1999a) found that high Fe^{3+} causes the 1.73 eV CL emission. In our samples however, we found no correlation between Fe concentration and the 1.73 eV band intensity. The lack of correlation may be explained by the fact that Fe occurs as divalent and trivalent ions. Fe^{2+} is assumed to produce no luminescence or act as luminescence quencher (*Marfunin*, 1979; *Götze*, personal communication, 2002).

Weak to non-luminescent, post-magmatic (secondary) quartz is depleted in Ti, Al, Fe and K (Figs. 7 and 8).

Discussion of geological implications

Topaz-bearing granites of the Hub stock hosting the Krásno Sn-W ore deposit contain three generations of igneous quartz, represented by phenocrysts (qz1), microphenocrysts (qz2), and groundmass quartz (qz3), indicating multiple crystallisation and varying crystallisation environments.

High Ti concentrations are typical for quartz formed at high temperatures ($>500\,^{\circ}C$) and pressure, such as in granulites (*Blankenburg* et al., 1994; *Van den Kerkhof* and *Müller*, 1999). Interpretation of Ti variation of growth zones in the phenocrysts (qz1 and qz2) requires distinction between zoning caused by self-organised growth and zoning caused by physico-chemical changes of external factors, such as temperature, pressure, and magma composition (e.g. *Allègre* et al., 1981; *Anderson*, 1984; *Fowler*, 1990; *Shore* and *Fowler*, 1996). Fine-scale oscillatory zoning arises from self-organised growth without the intervention of externally imposed periodicities in the state (pressure, temperature, or composition) of the melt from which the crystal grew (e.g., *Sibley* et al., 1976; *Allègre* et al., 1981; *Ortoleva*, 1990; *Shore* and *Fowler*, 1996). Self-organisation of growth is controlled by cyclic competition between the crystal growth rate and the diffusion rate of silica and other elements, such as Ti, within the crystal-melt reaction zone and boundary layer. In contrast, step zoning and resorption surfaces are zoning patterns

typically caused by variations in external factors (e.g., *Bottinga* et al., 1966; *Allègre* et al., 1981). Step zones are often bordered by resorption surfaces, which form round interior zone boundaries and truncate pre-existing growth zones (Figs. 4c and 5c). Resorption (melting) of quartz crystal surfaces indicates local SiO_2-undersaturation of the melt, which may be caused by (1) isothermal decompression due to magma ascent, or by (2) increase in temperature due to (2a) magma mixing or (2b) crystal settling, or by combination of (2a) and (2b):

(1) Isothermal decompression during adiabatic magma ascent can cause large-scale resorption of quartz crystals (e.g., *Johannes* and *Holtz,* 1996). Such adiabatic conditions are confined to rapid magma ascent in dykes. Resorption lowers the amount of suspended solids in the melt and thus the flow rate is elevated by a slight reduction of the effective viscosity (e.g., *Lejeune* and *Richet*, 1995). Ascent may be initiated by extension or shear in the upper crust. A suitable extensional regime was activated during the late-Variscan orogenic collapse, the time of extensive granite intrusions. The occurrence of resorption surfaces corresponds to the rapid ascent of granitic magmas by dyke formation as observed by *Clemens* and *Mawer* (1992), *Petford* (1996), *Johannes* and *Holtz* (1996), and *Clemens* et al. (1997). After a resorption episode (a presumed adiabatic magma ascent), the subsequent growth of a new zone starts with high Ti concentration (blue CL). The Ti contents decrease during further growth. In the case of adiabatic magma ascent, the initial high Ti incorporation can only be explained by a faster growth rate as the magma moved into cooler surroundings. High energy is necessary to incorporate Ti in quartz; this contradicts the assumption that Ti contents within quartz increase with progressing crystal growth rate.

(2a) The continuous whole rock fractionation trend of the granites of the Hub Stock and Krásno area (e.g., *Jarchovský* and *Pavlů*, 1991; *Breiter* et al., 1999) gives no indication of magma mixing. However, if the percentage of mafic melt input into the granite melt reservoir is very low, it is hard to proove mixing events on the basis of whole rock chemistry. Recent studies of feldspar phenocrysts show that magma mixing is widespread in late-Variscan granitic batholiths in central Europe (*Müller* and *Seltmann*, 2002; *Słaby* and *Galbarczyk-Gąsiorowska*, 2002). Therefore, multiple influx of a more mafic magma into the granite magma reservoir could be the cause of resorption episodes archived in the phenocryst growth pattern.

(2b) The density of quartz ($\sim 2.65 \cdot 10^3\,\mathrm{kg\,m^{-3}}$) would have been higher than the density of the granitic melt, which was less than $2.62 \cdot 10^3\,\mathrm{kg\,m^{-3}}$ (average density of solidified topaz-bearing granites in the Eastern Erzgebirge; *Kopf*, 1961), when the melt contained volatiles. Therefore, quartz crystal settling may also cause quartz solution if the crystal moves into a more silica-poor environment within a zoned magma reservoir. The melt inclusion gas-saturation pressure for CO_2 in samples from the Bishop Tuff increases from quartz phenocryst core to rim *(Anderson* et al., 2000). They assume that quartz crystal settling caused the increase in gas-saturation pressure and argue that some large quartz phenocrysts sank several kilometres through the zoned body of the Bishop Tuff magma. The outer rims of the phenocrysts which

overgrow an earlier resorption surface (see Fig. 5 in *Peppard* et al., 2001) show blue CL (*Anderson*, personal communication, 2002) and are enriched in Ti (see Table 1 in *Peppard* et al., 2001). Thus, both the increase in temperature and pressure favour the uptake of Ti into the quartz lattice. *Peppard* et al. (2001) stated that quartz phenocrysts grew as they sank, which is plausible because crystal settling is a relatively slow process and does not imply drastic changes in crystallisation conditions.

In conclusion, quartz resorption resulting in round surfaces was caused by magma dynamics produced either by influx of mafic magma into the granite magma reservoir or by large-scale crystal settling whereby large portions of the phenocrysts were moved into a more silica-poor environment in a zoned magma reservoir. We favour the first process, since recent studies (*Müller* and *Seltmann*, 2002; *Słaby* and *Galbarczyk-Gąsiorowska*, 2002) show that multiple influx of mafic magmas into the granite melt reservoir seems to be important during the extensional tectonics of the late-Variscan orogenic collapse. Moreover, magma mixing leads to increases in gas-saturation pressure, temperature, and Ti concentration of the magma, which initially cause the resorption of quartz and later (after local equilibration) the uptake of Ti into the quartz lattice. However, resorption which results in the final rounding of quartz phenocrysts observed in effusive silica-rich rocks (e.g., *Watt* et al., 1997) may be caused by adiabatic magma ascent.

Growth zoning and CL properties of qz1 and qz2 in the topaz granites are generally similar to those observed in phenocrysts of rhyolites, and particularly to those in the Permocarboniferous rhyolites of the Krušné Hory/Erzgebirge (*Müller* et al., 2001; Fig 5f). *Thomas* (1992) calculated the maximum depth of quartz phenocryst crystallisation in topaz-bearing granites from the Krušné Hory/Erzgebirge as 25 km, based on microthermometric studies of silicate melt inclusions. This agrees with the crystallisation depth of quartz phenocrysts in Permocarboniferous rhyolites of the Krušné Hory/Erzgebirge (*Thomas*, 1992). Moreover, most of the late-Variscan granites also contain zoned phenocrysts (*Müller* et al., 2000, 2001, 2002a) originating from the same depth (*Thomas,* 1992). Estimations of water contents of melt inclusions in phenocrysts of granites from the Western Krušné Hory/Erzgebirge by *Thomas* and *Klemm* (1997) reveal 3–4 equiv.-wt% H_2O, which corresponds to a relative water-poor crystallisation environment. The late-Variscan granites and rhyolites of the Krušné Hory/Erzgebirge intruded and extruded, respectively, over a period of about 40 Ma (e.g., *Förster* et al., 1999; *Breiter* et al., 1999). The similarities discussed imply the presence of a long-standing, partly interconnected magma stockwork beneath the Krušné Hory/Erzgebirge region, which has been a matter of debate since *Watznauer* (1954). The magma stockwork probably consists of several spatially and temporally separated sub-reservoirs, because the growth pattern and trace element signature of quartz phenocrysts differ slightly between the granites of the Krušné Hory/Erzgebirge (*Müller* et al., 2000, 2002a). Another indication for the long-standing magma stockwork is the occurrence of old (inherited) granitic zircons with an age of about 330 Ma (Pb/Pb single zircon, *Kempe* et al., 1999b) in the younger Altenberg-Frauenstein microgranite (Eastern Krušné Hory/Erzgebirge),

which is dated at 307–309 Ma (Ar/Ar plateau ages of unaltered biotite, *Seltmann* and *Layer*, unpubl., in *Seltmann* and *Schilka*, 1995).

The groundmass quartz (qz3) crystallised during and after the magma emplacement at about 1.5 km depth (*Thomas*, 1994). The higher Al in the groundmass quartz may reflect the increase of water (6–9 wt% H_2O according to *Thomas* and *Klemm*, 1997) and of lithophile elements Al^{3+}, K^+, Na^+, and Li^+ in the late-stage melt, because Al forms water-bearing [$2SiO_3$–H_2O–M^+–$2AlO_4$] defect cluster, where M^+ is K^+, Na^+, or Li^+ (*Müller* et al., 2002a).

Conclusions

We demonstrated that EPMA is well suited for the study of Al and Ti in zoned quartz crystals. The zoning of quartz phenocrysts from the topaz granites imaged with CL shows a clear association with the Ti distribution in quartz. We thus conclude that most of the Ti analysed is structurally incorporated. On the other hand Al in igneous quartz shows no obvious correlation with CL.

The zoned phenocrysts in the topaz granites with dominant blue CL and high average Ti crystallised from a water-poor (~3 wt% H_2O) magma in the lower to middle crust. Such phenocrysts record the early stages of magma evolution, and show features similar to phenocrysts in rhyolites. The occurrence of zoned quartz phenocrysts in most of the late-Variscan granites of the Krušné Hory/Erzgebirge, which are similar to the phenocrysts in the Hub stock granites, implies that a long-standing magma stockwork with several spatialy and temporaly separated sub-reservoirs existed beneath the Krušné Hory/Erzgebirge region. During the collapse of the Variscan orogen the magmas of this stockwork ascended along extensional structures.

The study shows that quartz is a resistant and generally underestimated archivist of magma evolution.

Acknowledgements

We are indebted to *A.M. van den Kerkhof, R. Seltmann, J. Gardner, C. Stanley* and *U. Hein* for discussion and critical comments. The research has been supported by the Deutsche Forschungsgemeinschaft (DFG) through grant MU 1717/2-1 and by the European Commission's Improving Human Potential (IHP) programme within the SYS-RESOURCE award scheme providing access to the facilities of The Natural History Museum, London.

References

Allègre CJ, Provost A, Jaupart C (1981) Oscillatory zoning: a pathological case of crystal growth. Nature 294: 223–228

Anderson AT (1984) Probable relations between plagioclase zoning and magma dynamics, Fuego Volcano, Guatemala. Am Mineral 69: 660–676

Anderson AT, Davis AM, Lu F (2000) Evolution of Bishop Tuff rhyolitic magma based on melt and magnetite inclusions and zoned phenocrysts. J Petrol 41: 449–473

Armstrong JT (1991) Quantitative elemental analysis of individual microparticles with electron beam instruments. In: *Heinrich KFJ, Newbury DE* (eds) Electron probe quantification. Plenum Press, New York London, pp 261–315

Armstrong JT (1995) CITZAF: A package of correction programs for the quantitative electron microbeam x-ray analysis of thick polished materials, thin films, and particles. Microbeam Analysis 4/1995: 177–200

Bahadur H (1993) Hydroxyl defects and electrodiffusion (sweeping) in natural quartz crystals. J Appl Phys 73(11): 7790–7797

Bambauer HU (1961) Spurenelementgehalt und Farbzentren in Quarzen aus Zerrklüften der Schweizer Alpen. Schweiz Mineral Petrogr Mitt 43: 259–268

Bambauer HU, Brunner GO, Laves F (1963) Merkmale des OH-Spektrums alpiner Quarze (3 μ-Gebiet). Schweiz Mineral Petrogr Mitt 41: 335–369

Blankenburg HJ, Götze J, Schulz J (1994) Quarzrohstoffe. Deutscher Verlag für Grundstoffindustrie, Leipzig Stuttgart, 296 pp

Bottinga Y, Kudo A, Weill D (1966) Some observations on oscillatory zoning and crystallisation of magmatic plagioclase. Am Mineral 51: 792–806

Breiter K, Förster HJ, Seltmann R (1999) Variscan silicic magmatism and related tin-tungsten mineralization in the Erzgebirge-Slavkovský Les metallogenic province. Mineral Deposita 34: 505–521

Clemens JD, Mawer CK (1992) Granitic magma transport by fracture propagation. Tectonophysics 204: 339–360

Clemens JD, Petford N, Mawer CK (1997) Ascent mechanisms of granitic magmas: causes and consequences. In: *Holness MB* (ed) Deformation-enhanced fluid transport in the Earth's crust and mantle. Mineral Soc Series 8: 145–172

D'Lemos RS, Kearsley AT, Pembroke JW, Watt GR, Wright P (1997) Complex quartz growth histories in granite revealed by scanning cathodoluminescence techniques. Geol Mag 134: 459–552

Dennen WH (1965) Stoichiometric substitution in natural quartz. Geochim Cosmochim Acta 30: 1235–1241

Fiala F (1968) Granitoids of the Slavkovský Les Mountains. Sbor geol Vìd G 14: 93–160

Flem B, Larsen RB, Grimstvedt A, Mansfeld J (2002) In situ analysis of trace elements in quartz by using laser ablation inductively coupled plasma mass spectrometry. Chem Geol 182: 237–247

Förster HJ, Tischendorf G, Seltmann R, Gottesmann B (1999) Die variszischen Granite des Erzgebirges: neue Aspekte aus stofflicher Sicht. Z geol Wissensch 26: 31–60

Fowler AD (1990) Self-organized mineral textures of igneous rocks: the fractal approach. Earth Sci Rev 29: 47–55

Frondel C (1934) Origin of the segmental coloration of amethyst and smoky quartz. Am Mus Novitates 758: 1–15

Götze J (2000) Cathodoluminescence microscopy and spectroscopy in applied mineralogy. Freiberger Forschungsh C485: 128 pp

Götze J, Plötze M, Habermann D (2001) Origin, spectral characteristics and practical applications of the cathodoluminescence (CL) of quartz: a review. Mineral Petrol 71: 225–250

Griscom DL (1985) Defect structures of glass. J Non-Cryst Solids 73: 51–77

Holness MB, Watt GR (2001) Quartz crystallization and fluid flow during contact metamorphism: a cathodoluminescence study. Geofluids 1: 215–228

Jarchovský T (2001) Sn-W mineralization in the Krásno district. In: *Breiter K* (ed) Phosphorus- and fluorine-rich fractionated granites. International Workshop 16.–19. 10. 2001, Podlesí, Czech Republic, Czech Geological Survey, pp 79–98

Jarchovský T, Pavlů D (1991) Albite-topaz microgranite from Horní Slavkov (Slavkovský Les Mts.) North Bohemia. Věst Ústř úst geol 66: 13–22

Jarchovský T, Pavlů D, Morysek J, Najman K, Kozubek P (1994) Li-F granite cupolas and Sn-W mineralization in the Slavkovský Les Mts., Czech Republic. Monogr Series Mineral Deposits 31: 131–148

Johannes W, Holtz F (1996) Petrogenesis and experimental petrology of granitic rocks. Springer, Berlin Heidelberg New York Tokyo, 335 pp

Kempe U, Götze J, Dandar S, Habermann D (1999a) Magmatic and metasomatic processes during formation of the Nb-Zr-REE deposits from Khaldzan Buregte (Mongolian Altai): indications from a combined CL-SEM study. Mineral Mag 63: 165–177

Kempe U, Wolf D, Ebermann U, Bombach K (1999b) 330 Ma Pb/Pb single zircon evaporation ages for the Altenberg Granite Porphyry, Eastern Erzgebirge (Germany): implications for Hercynian granite magmatism and tin mineralisation. Z geol Wissensch 27: 385–400

Kopf M (1961) Dichtewerte von Gesteinen des Erzgebirges und der angrenzenden Gebiete. Z Angew Geol 6: 301–302

Kozlowski A (1981) Melt inclusions in pyroclastic quartz from the Carboniferous deposits of the Holy Cross Mts, and the problem of magmatic corrosion. Acta Geol Polonica 31: 273–283

Kronenberg AK, Kirby SH, Aines RD, Rossmann GR (1986) Solubility and diffusional uptake of hydrogen in quartz at high water pressures: implications for hydrolytic weakening in the laboratory and within the earth. Tectonophysics 172: 255–271

Laemmlein G (1930) Korrosion und Regeneration der Porphyr-Quarze. Z Kristallogr 75: 109–127

Lange H, Tischendorf G, Pälchen W, Klemm I, Ossenkopf W (1972) Zur Petrographie und Geochemie der Granite des Erzgebirges. Geologie 21: 457–493

Larsen RB, Polve M, Juve G (2000) Granite pegmatite quartz from Evje-Iveland: trace element chemistry and implications for the formation of high-purity quartz. Norges Geol Unders Bull 436: 57–65

Lehmann G (1975) On the colour centres of iron in amethyst and synthetic quartz: a discussion. Am Mineral 60: 335–337

Lehmann G, Bambauer HV (1973) Quarzkristalle und ihre Farben. Angew Chem 7: 281–289

Lejeune AM, Richet P (1995) Rheology of crystal-bearing silicate melts: an experimental study at high viscosities. J Geophys Res 100: 4215–4230

Lowenstern JB (1995) Applications of silicate-melt inclusions to the study of magmatic volatiles. In: *Thompson JFH* (ed) Magmas, fluids and ore deposits. Mineral Assoc Canada Short Course 23: 71–99

Lowenstern JB, Sinclair WD (1996) Exsolved magmatic fluid and its role in the formation of comb-layered quartz at the Cretaceous Logtung W-Mo deposit, Yukon Territory, Canada. Trans Roy Soc Edinburgh. Earth Sci 87: 291–303

Marfunin AS (1979) Spectroscopy, luminescence and radiation centers in minerals. Springer, Berlin Heidelberg New York, 345 pp

Marshall DJ (1988) Cathodoluminescence of geological materials. Allen & Unwin, Winchester/Mass, 146 pp

Maschmeyer D, Lehmann G (1983) New hole centres in natural quartz. Phys Chem Minerals 10: 84–88

Morgan GB, London D, Luedke RG (1998) Petrochemistry of late Miocene peraluminous silicic volcanic rocks from the Morococala field, Bolivia. J Petrol 39: 601–632

Müller A (2000) Cathodoluminescence and characterisation of defect structures in quartz with applications to the study of granitic rocks. Thesis, University Göttingen, 230 pp (unpublished)

Müller A, Seltmann R (1999) The genetic significance of snowball quartz in high fractionated tin granites of the Krušne Hory/Erzgebirge. In: *Stanley CJ* et al. (eds) Mineral deposits: processes to processing, vol 1. Balkema, Rotterdam, pp 409–412

Müller A, Seltmann R (2002) Plagioclase-mantled K-feldspar in the Carboniferous porphyritic microgranite of Altenberg-Frauenstein, Eastern Erzgebirge/Krušné Hory. Bull Geol Soc Finland 74: 53–79

Müller A, Seltmann R, Behr HJ (2000) Application of cathodoluminescence to magmatic quartz in a tin granite – case study from the Schellerhau Granite Complex, Eastern Erzgebirge, Germany. Mineral Deposita 35: 169–189

Müller A, Müller B, Behr H-J (2001) Structural contrasts in granitic rocks of the Lusatian Granodiorite Complex and the Erzgebirge, Germany – in commemoration of Hans Cloos. Z geol Wissensch 29: 521–544

Müller A, Kronz A, Breiter K (2002a) Trace elements and growth pattern in quartz: a fingerprint of the evolution of the subvolcanic Podlesí Granite System (Krušné Hory, Czech Republic). Bull Czech Geol Surv 77: 135–145

Müller A, Lennox P, Trzebski R (2002b) Cathodoluminescence and micro-structural evidence for crystallisation and deformation processes of granites in the Eastern Lachlan Fold Belt (SE Australia). Contrib Mineral Petrol 143: 510–524

Müller A, Wiedenbeck M, Van den Kerkhof AM, Kronz A, Simon K (2003) Trace elements in quartz – a combined electron microprobe, secondary ion mass spectrometry, laser-ablation ICP-MS, and cathodoluminescence study. Eur J Mineral (in press)

Mullis J, Ramseyer K (1999) Growth related Al-uptake in fissure quartz, Central Alps, Switzerland. Terra Nostra 99/6: 209

Neuser RD, Bruhn F, Götze J, Habermann D, Richter DK (1995) Kathodolumineszenz: Methodik und Anwendung. Zbl Geol Paläont Teil 1 1/2: 287–306

Ortoleva PJ (1990) Role of attachment kinetic feedback in the oscillatory zoning of crystals grown from melts. Earth Sci Rev 29: 3–8

Pagel M, Barbin V, Blanc P, Ohnenstetter D (2000) Cathodoluminescence in geosciences. Springer, Berlin Heidelberg New York Tokyo, 514 pp

Peppard BT, Steele IM, Davis AM, Wallace PJ, Anderson AT (2001) Zoned quartz phenocrysts from the rhyolitic Bishop Tuff. Am Mineral 86: 1034–1052

Perny B, Eberhardt P, Ramseyer K, Mullis J, Pankrath R (1992) Microdistribution of aluminium, lithium and sodium in a quartz: possible causes and correlation with shored lived cathodoluminescence. Am Mineral 77: 534–544

Petford N (1996) Dykes or diapirs? Trans Roy Soc Edinburgh Earth Sci 87: 104–114

Pott GT, McNicol BD (1971) Spectroscopic study of the coordination and valence of Fe and Mn ions in and on the surface of aluminas and silicas. Disc Faraday Soc 52: 121–131

Ramseyer K, Mullis J (1990) Factors influencing short-lived blue cathodoluminescence of α-quartz. Am Mineral 75: 791–800

René M (1998) Development of topaz-bearing granites of the Krudum massif (Karlovy Vary pluton). Acta Univ Carolinae Geol 42: 103–109

Rovetta MR, Blacic JD, Hervig RL, Holloway JR (1989) An experimental study of hydroxyl in quartz using infrared spectroscopy and ion microprobe techniques. J Geophys Res 94: 5840–5850

Schneider N (1993) Das lumineszenzaktive Strukturinventar von Quarzphänokristen in Rhyolithen. Göttinger Arb Geol Paläont 60: 81 pp

Schrön W, Schmädicke E, Thomas R, Schmidt W (1988) Geochemische Untersuchungen an Pegmatitquarzen. Z geol Wissensch 16: 229–244

Seltmann R (1994) Sub-volcanic minor intrusions in the Altenberg caldera and their metallogeny. In: *Seltmann R, Kämpf H, Möller P* (eds) Metallogeny of collosional orogens. Czech Geological Survey, Prague, pp 198–206

Seltmann R, Schilka W (1995) Late-Variscan crustal evolution in the Altenberg-Teplice Caldera. Evidence from new geochemical and geochronological data. Terra Nostra 7/95: 120–124

Seltmann R, Bankwitz P, Frischbutter A, Thomas R (1992) Metallogenic position of breccia-related granite bodies at the north-western border of the Bohemian Massif (Krušné Hory-Krásný Les area). In: *Kukal Z* (ed) Proc 1st Int Conf Bohemian Massif, Prague 1988. Czech Geol Surv, Prague, pp 257–268

Seyedolali A, Krinsley DH, Boggs S, O'Hara PF, Dypvik H, Goles GG (1997) Provenance interpretation of quartz by scanning electron microscope-cathodoluminescence fabric analysis. Geology 25: 787–790

Shimizu N, Semet MO, Allègre CB (1978) Geochemical applications of quantitative ion-microprobe analysis. Geochim Cosmochim Acta 42: 1321–1334

Shore M, Fowler AD (1996) Oscillatory zoning in minerals: a common phenomenon. Can Mineral 34: 1111–1126

Sibley DF, Vogel TA, Walker BM, Byerly G (1976) The origin of oscillatory zoning in plagioclase: a diffusion and growth controlled model. Am J Sci 276: 275–284

Siegel GH, Marrone MJ (1981) Photoluminescence in as-drawn and irradiated silica optical fibers: an assessment of the role of non-bridging oxygen defect centres. J Non-Cryst Solids 45: 235–247

Słaby E, Galbarczyk-Gąsiorowska L (2002) Barium in alkali feldspar megacrysts from Szklarska Poręba Huta porphyritic granite: possibly indicator of magma mixing. Mineral Soc Poland, Spec Papers 20: 198–200

Sprunt E (1981) Causes of quartz cathodoluminescence colours. Scan Electron Micr 1981: 525–535

Stenina NG (1995) Energy aspect in the formation of granitic magma and ore deposits. In: *Pašava J, Křibek B, Žák K* (eds) Mineral deposits: from their origin to their environmental impacts. Balkema, Rotterdam, pp 539–542

Stenina NG, Sotnikov VI, Korolyuk VN, Kovaleva LT (1988) Microstructural features of hydrothermal vein quartz as an indicator of mineralization. Geokhimiya 5: 641–653 (English translation)

Stevens Kalceff MAS, Phillips MR (1995) Cathodoluminescence microcharacterisation of the defect structure of quartz. Phys Rev B 52: 3122–3134

Suttner LJ, Leininger RK (1972) Comparison of the trace element content of plutonic, volcanic, and metamorphic quartz from southwestern Montana. Geol Soc Am Bull 83: 1855–1862

Thomas R (1992) Results of investigations on melt inclusions in various magmatic rocks from the northern border of the Bohemian Massif. In: *Kukal Z* (ed) Proc 1st Int Conf Bohemian Massif, Prague 1988. Czech Geol Survey, Prague, pp 298–306

Thomas R (1994) Fluid evolution in relation to the emplacement of the Variscan granites in the Erzgebirge region: a review of the melt and fluid inclusion evidence. In: *Seltmann R, Kämpf H, Möller P* (eds) Metallogeny of collosional orogens. Czech Geological Survey, Prague, pp 70–81

Thomas R, Klemm W (1997) Microthermometric study of silicate melt inclusions in Variscan granites from SE Germany: volatile contents and entrapment conditions. J Petrol 38: 1753–1765

Van den Kerkhof AM, Müller A (1999) Fluid inclusion re-equilibration and trace element redistribution in quartz: observations by cathodoluminescence. ECROFI XV Abstracts and Program, Terra Nostra 99/6: 161–162

Van den Kerkhof AM, Kronz A, Simon K (2001) Trace element redistribution in metamorphic quartz and fluid inclusion modification: observations by cathodoluminescence. XVI ECROFI, Fac Ciências Porto, Dep Geol Memória 7: 447–450

Watt GR, Wright P, Galloway S, McLean C (1997) Cathodoluminescence and trace element zoning in quartz phenocrysts and xenocrysts. Geochim Cosmochim Acta 61: 4337–4348

Watznauer A (1954) Die erzgebirgischen Granitintrusionen. Geologie 3: 688–706

Waychunas GA (1988) Luminescence, X-ray emission and new spectroscopies. In: *Hawthrone FC* (ed) Spectroscopic methods in mineralogy and geology. Rev Mineral 18: 639–698

Weil JA (1984) A review of electron spin spectroscopy and its application to the study of paramagnetic defects in crystalline quartz. Phys Chem Minerals 10: 149–165

Authors' addresses: *A. Müller*, Department of Mineralogy, Natural History Museum, Cromwell Road, London SW7 5BD, United Kingdom, e-mail: a.mueller@nhm.ac.uk; *M. René*, Institute of Rock Structure and Mechanics, Academy of Sciences of the Czech Republic, V Holešovičkách 41, 182 09 Prague 8, Czech Republic, e-mail: rene@irsm.cas.cz; *H.-J. Behr* and *A. Kronz* (e-mail: akronz@gwdg.de), GZG, Goldschmidtstrasse 3, D-37077 Göttingen, Germany